Journal of Nuclear Materials 538 (2020) 152195

Contents lists available at ScienceDirect

Journal of Nuclear Materials

journal homepage: www.elsevier.com/locate/jnucmat

Modeling intra-granular fission gas bubble evolution and coarsening in uranium dioxide during in-pile transients

T. Barani [a], G. Pastore [b, d], A. Magni [a], D. Pizzocri [a], P. Van Uffelen [c], L. Luzzi [a, *]

[a] Politecnico di Milano, Department of Energy, Nuclear Engineering Division, Via La Masa 34, I-20156, Milano, Italy
[b] Idaho National Laboratory, Computational Mechanics and Materials Department, P.O. Box 1625, Idaho Falls, ID, 83415-3840, United States
[c] European Commission, Joint Research Centre, Directorate for Nuclear Safety and Security, P.O. Box 2340, 76125, Karlsruhe, Germany
[d] University of Tennessee, Department of Nuclear Engineering, 1412 Circle Dr, Knoxville, TN 37916, United States

ARTICLE INFO

Article history:
Received 23 January 2020
Received in revised form
11 April 2020
Accepted 23 April 2020
Available online 2 June 2020

Keywords:
Fission gas behavior
Intra-granular behavior
Bubble coarsening
Oxide fuel
Gaseous swelling
Fuel performance codes

ABSTRACT

The description of intra-granular fission gas behavior during irradiation is a fundamental part of models used for the calculation of fission gas release and gaseous swelling in nuclear fuel performance codes. The relevant phenomena include diffusion of gas atoms towards the grain boundaries coupled to the evolution of intra-granular bubbles. While intra-granular bubbles during normal operating conditions are limited to sizes of a few nanometers, experimental evidence exists for the appearance of a second population of bubbles during transients, characterized by coarsening to sizes of tens to hundreds of nanometers and that can significantly contribute to gaseous fuel swelling. In this work, we present a model of intra-granular fission gas behavior in uranium dioxide fuel that includes both nanometric fission gas bubble evolution and bubble coarsening during transients. While retaining a physical basis, the developed model is relatively simple and is intended for application in engineering fuel performance codes. We assess the model through comparisons to a substantial number of experimental data from SEM observations of intra-granular bubbles in power ramp tested uranium dioxide samples. The results demonstrate that the model reproduces the coarsening of a fraction of the intra-granular bubbles and correspondingly, predicts gaseous swelling during power ramps with a significantly higher accuracy than is allowed by traditional models limited to the evolution of nanometric intra-granular bubbles.

1. Introduction

The behavior of the gaseous fission products xenon and krypton significantly affects the performance of nuclear fuel rods during irradiation [1,2]. Gas atoms are created in the fuel grains during fission events and due to their low solubility, tend to precipitate forming bubbles. Intra-granular bubble evolution is governed by gas atom trapping from the matrix into the bubbles and the counteracting mechanism of irradiation-induced re-solution of gas atoms from the bubbles back into the matrix. Concomitantly, diffusion to grain boundaries of atoms dissolved in the matrix occurs [3–8]. The behavior of gas at grain boundaries determines inter-granular gaseous swelling and fission gas release to the rod free volume [2,8]. Although inter-granular swelling due to grain-boundary bubbles is the dominant contribution to gaseous fuel swelling under normal operating conditions, intra-granular swelling becomes significant during transients to high temperatures and at high burnups [9–14].

During normal operating conditions, intra-granular fission gas bubbles are generally limited to sizes of one to a few nanometers [15]. However, experiments have shown the appearance of a second population of bubbles characterized by sizes of tens to hundreds of nanometers, which has been observed following post-irradiation annealing, power ramps and in high-burnup fuel [9–18]. Although the mechanisms for such abnormal bubble growth are largely unknown (see, e.g. Refs. [14,15,17,18]), there is evidence that the larger bubbles are associated with dislocations [9,10,14,19]. The population of larger bubbles can account for local gaseous swelling of up to 7–8% volumetric fraction [13,14,16] and is therefore of high engineering interest.

* Corresponding author.
E-mail addresses: tommaso.barani@polimi.it (T. Barani), giovanni.pastore@inl.gov (G. Pastore), alessio.magni@polimi.it (A. Magni), davide.pizzocri@polimi.it (D. Pizzocri), paul.van-uffelen@ec.europa.eu (P. Van Uffelen), lelio.luzzi@polimi.it (L. Luzzi).

https://doi.org/10.1016/j.jnucmat.2020.152195

Nomenclature

α_b	Re-solution rate of atoms from bulk bubbles (s^{-1})
α_d	Re-solution rate of atoms from dislocation bubbles (s^{-1})
β'	Trapping rate at dislocations (s^{-1})
β_b	Trapping rate at bulk bubbles (s^{-1})
β_d	Trapping rate at dislocation bubbles (s^{-1})
δ	Wigner-Seitz radius associated to a dislocation bubble (m)
δ_{HS}	Hard sphere diameter of a xenon atom (m)
$\frac{\Delta V_f}{V_f}$	Gaseous fuel swelling (/)
η	Number of bubbles nucleated per fission fragment (bubble per fission fragment)
γ	UO_2-bubble surface energy ($J\ m^{-2}$)
ν_b	Nucleation rate of bubbles in the bulk ($m^{-3}\ s^{-1}$)
ν_d	Nucleation rate of bubbles at dislocations ($m^{-3}\ s^{-1}$)
Ω	Volume of a vacancy (m^3 vacancy^{-1})
ω	Volume of a gas atom (m^3 atom^{-1})
ρ_d	Space-averaged dislocation density ($m\ m^{-3}$)
σ_h	Hydrostatic stress (Pa)
ν	Atomic density in dislocation bubbles (atom m^{-3})
$\tilde{y}$	Packing fraction in the Hard Sphere equation of state (/)
ζ	Sink strength of a dislocation bubble (/)
B	Volume of a gas atom into bulk bubbles (m^3 atom^{-1})
b	Burgers vector magnitude in UO_2 (m)
c	Concentration of single gas atoms in the matrix (atom m^{-3})
D	Single gas atom bulk diffusion coefficient ($m^2\ s^{-1}$)
D_d	Single gas atom diffusion coefficient close to the dislocation core ($m^2\ s^{-1}$)
$D_{i,bulk}$	Bulk diffusion coefficient of interstitials ($m^2\ s^{-1}$)
D_i	Interstitial diffusion coefficient along the dislocation core ($m^2\ s^{-1}$)
$D_{v,bulk}$	Bulk diffusion coefficient of vacancies ($m^2\ s^{-1}$)
D_v	Vacancy diffusion coefficient along the dislocation core ($m^2\ s^{-1}$)
F	Fission rate density fission ($m^{-3}\ s^{-1}$)
K	Number of bubbles nucleated per dislocation (bubble m^{-1})
k	Boltzmann constant ($J\ K^{-1}$)
m_b	Concentration of gas atoms in bulk bubbles (atom m^{-3})
m_d	Concentration of gas atoms in dislocation bubbles (atom m^{-3})
N_b	Number density of bulk bubbles (bubble m^{-3})
n_b	Number of atoms per bulk bubble (atom bubble^{-1})
N_d	Number density of bubbles at dislocations (bubble m^{-3})
n_d	Number of atoms per dislocation bubble (atom bubble^{-1})
n_v	Number of vacancies per dislocation bubble (vacancy bubble^{-1})
p	Pressure of dislocation bubbles (Pa)
p_{eq}	Equilibrium pressure of dislocation bubbles (Pa)
R_b	Radius of bulk bubbles (m)
R_d	Radius of dislocation bubbles (m)
r_d	Effective dislocation core radius (m)
$r_{ws,d}$	Wigner-Seitz cell radius associated with a dislocation (m)
T	Temperature (K)
V_b	Volume of a bulk bubble (m^3)
V_d	Volume of a dislocation bubble (m^3)
y	Yield of gas atoms per fission event (atom fission^{-1})

Given the importance of fission gas behavior (FGB) in fuel rod performance, models for fission gas release and gaseous fuel swelling have been developed and incorporated in engineering fuel performance codes [5,8,13,20–30]. However, these models are generally limited to the evolution of nanometric bubbles [5,21,24,26,28–30]. Developing models able to represent the bubble coarsening (i.e., abnormal growth) effect and that can be effectively applied in fuel performance codes appears necessary in order to accurately model fuel behavior in high temperature transients and high-burnup conditions. Modeling fuel gaseous swelling during transients such as power ramps has implications, for example, in the analysis of pellet-cladding interaction (PCI) [31].

In engineering fuel performance calculations, fission gas models are called, for each time step and each non-linear iteration, in every element of the computational mesh, thus they need to be computationally efficient. The authors previously developed models to calculate fission gas release and gaseous swelling in UO_2 [27,30,32,33], which constitute the foundation of mechanistic FGB calculations in the TRANSURANUS and BISON fuel performance codes [34–37]. In particular, in Refs. [30] a model for intra-granular fission gas behavior was developed. The model is limited to the evolution of nanometric fission gas bubbles during normal operating conditions and represents the bubble size distribution with the mean size and the total number density ('single-size' model). In this work, we extend the description of intra-granular FGB presented in Ref. [30] to consider bubble evolution and coarsening during high-temperature transients in addition to behavior during normal operating conditions.

A model for bubble coarsening under post-irradiation annealing conditions was proposed by White [13]. In particular, White considered the role of the dislocation network in the fuel acting as a vacancy sink or a vacancy source, with vacancy absorption at intra-granular bubbles being dependent on the dislocation density. White's model only covered annealing conditions and the population of coarsened bubbles visible through Scanning Electron Microscopy (SEM), without consideration of bubble nucleation and re-solution. A purely empirical model of intra-granular bubble coarsening was proposed by Lösönen [18,21]. In this model, coarsening was triggered at the attainment of a temperature threshold, with the average bubble radius during coarsening being calculated as a function of time with an exponential relation leading to a (fixed) saturation value of 100 nm. Mechanistic modeling of intra-granular bubble coarsening under irradiation was considered by Veshchunov and coworkers [24,28,38]. In this case, bubble coarsening during transients was ascribed to bubble-size dependent re-solution of fission gas atoms from bubbles. In particular, as re-solution becomes less effective with increasing bubble radius, it was postulated that a fraction of the bubbles may surmount a 'critical' size beyond which they are able to further grow without significant restriction.

The model developed in the present work considers the reduced effectiveness of re-solution with increasing bubble radius on the basis of atomic-scale calculations but invokes the role of dislocations as a source of vacancies and preferential growth along dislocations as the mechanism for bubble coarsening. The model computes the average size and number density of both populations

of nanometric bubbles in the fuel bulk and coarsening bubbles along dislocations, the corresponding gaseous fuel swelling, and diffusion of single gas atoms to grain boundaries which is coupled to bubble evolution. While both nanometric and coarsening bubbles are modeled, only the average size of each population is considered. In this sense, the new model can be considered as a 'two-size' description of intra-granular bubble evolution.

The model presented in this work integrates information obtained from atomistic calculations for the parameters (in particular, for re-solution rate and defect diffusivities). Yet, it is meant for inclusion in engineering-scale fuel performance codes, thus retains a focus to end-user, industrial applications.

Model predictions, in terms of bubble size, number density and gaseous swelling, are compared to the extensive experimental database of White and coworkers [14], consisting in SEM observations of power ramp tested UO_2 samples.

The outline of the paper is as follows. In Section 2, we discuss the physical processes considered for fission gas behavior and the related modeling, including the developed theory for bubble coarsening. In Section 3, we present the general formulation of the intra-granular FGB model. In Section 4, we present the comparison of model predictions to experimental data. Conclusions are drawn in Section 5.

2. Physical processes

2.1. General considerations

The in-pile evolution of intra-granular bubbles in oxide nuclear fuels is mainly governed by the following processes: bubble nucleation, irradiation-induced re-solution of gas atoms from the bubbles back into the lattice, absorption of gas atoms (trapping) and vacancies at bubbles, and bubble coalescence.

During normal operating conditions, intra-granular bubbles generally have number densities of the order of $10^{23} - 10^{24}$ m^{-3}, spherical and/or faceted shape,[1] diameters of one to a few nanometers, and a gas density of 3–7 g cm^{-3} [17,19,41–45], close to the density of solid-state Xe (e.g. Refs. [5,6,15,19,45]). In these conditions, intra-granular bubbles are strongly overpressurized, as concluded by authors analyzing fuels irradiated in commercial light water reactors up to 80 GWdt^{-1} [43,46]. The over-pressurization and small size of intra-granular bubbles during normal operating conditions has been ascribed to a 'vacancy starvation' effect, which has been postulated for UO_2 under both irradiation and annealing[2] conditions [13,46,49,50].

During high-temperature transient and high-burnup[3] conditions, while the population of nanometric bubbles is still present, a second population of coarsened bubbles with lower number densities and larger sizes of tens to hundreds of nanometers has been observed [9–14]. Coarsened bubbles can be associated with significant fuel gaseous swelling [13,14,16]. This selective bubble growth under certain conditions suggests that a threshold process exists for the activation of significant absorption of vacancies at a fraction of the bubbles.

We refer to the abnormal growth of a fraction of the intra-granular bubbles as bubble *coarsening*. When dealing with a diluted phase in a two-phase system, this term is usually adopted in the literature in reference to the growth of larger particles absorbing solute atoms which are made available by smaller particles [51–53]. This process, known as Ostwald ripening, has been considered by several authors to describe the growth of gas bubbles and voids in nuclear materials (e.g. Ref. [54–59]). While we refer to the abnormal intra-granular bubble growth adopting the same terminology, we do not consider Ostwald ripening as the phenomenon responsible for abnormal growth of intra-granular bubbles during irradiation, as we detail in the following.

Mechanisms that have been proposed for bubble coarsening under in-pile and annealing conditions include bubble coalescence through bubble migration due to surface or volume diffusion, and Ostwald ripening [11,15,28,54–56]. An additional mechanism of bubble growth has been investigated by molecular dynamics employing empirical pair potentials by Murphy and co-workers [60]. They suggest that nanometric intra-granular bubbles would force the surrounding oxygen ions into the lattice to relieve the internal pressure. Even though this mechanism may contribute to relaxing the bubble internal pressure, we consider that further evidence is needed before it can be regarded as a primary contribution to bubble coarsening.

As for bubble migration either via surface or volume diffusion, from a theoretical perspective, the effectiveness of both phenomena in UO_2 under irradiation is drastically reduced at bubble radii exceeding $\approx$10 nm [28,47,61,62] This is due to the dependence of volume and surface diffusivities on the bubble radius, with diffusivities being proportional to R_b^{-3} and R_b^{-4} [47], respectively. Moreover, the activation energy of cations in UO_2 is deemed too high to cause an appreciable volume diffusion mechanism [28]. Also, various mechanisms of surface diffusion suppression under irradiation have been elucidated in the literature [15,47]. Ostwald ripening involves a transfer of gas atoms from small bubbles to larger ones. This mechanism is inhibited if the bubbles are strongly overpressurized [15,54,56], as is the case for the nanometric bubbles in UO_2 grains experiencing the vacancy starvation condition. Moreover, Ostwald ripening involves (thermal) re-solution of gas atoms from small bubbles being transferred to larger ones. Thermal re-solution would entail high solubility of gaseous fission products in the UO_2 crystal, to enable a substantial flux of gas atoms from the small bubbles to the larger ones. On one hand, xenon should retain a non-zero solubility in the crystal matrix close to intra-granular bubbles and its solubility should increase with temperature and bubble over-pressurization. On the other, the expected low value of solubility prevents a substantial thermal re-solution to take place [60,63,64]. Lastly, in-pile experimental intra-granular bubble size distributions reported in Ref. [14] exhibit a right skewness which is not compatible with Ostwald ripening effects (cf. [53]). Nevertheless, it must be noted that in high temperature annealing experiments on irradiated UO_2 Ostwald ripening may play a role in the coarsening of intra-granular bubbles, together with vacancy-assisted migration and coalescence (e.g. Refs. [11,13,38,47,59,65]). In fact, grain boundaries in these conditions may act as source of thermal vacancies for the intra-granular bubble population. Nevertheless, the focus of the model presented in this paper is on in-pile transients.

The observations of coarsened bubbles being along dislocations [9,10,14,19] suggest a role of dislocations in favoring selected bubble growth under certain conditions. It is accepted that fission gas bubbles at grain boundaries grow to micrometric sizes through vacancy absorption (e.g. Ref. [23]), which is favored at grain boundaries compared to the bulk of the fuel. Bubble growth due to vacancy absorption at grain boundaries driven by bubble overpressure has been broadly considered in modeling inter-granular

[1] In UO_2, faceted bubbles have been observed by a few authors (e.g. Ref. [39,40]), especially when the radii reach values of multiple nanometers.

[2] An exception is represented by the evolution during annealing tests of intra-granular bubbles located near grain boundaries, which can act as a source of thermal vacancies, allowing for localized bubble coarsening and/or vacancy-assisted migration [11,47,48].

[3] Here, we do not refer to the inter-granular porosity developing at the periphery of light water reactor fuels at high burnup. Instead, we refer to the intra-granular bubble population in the non-restructured fuel irradiated up to high burnups.

fission gas behavior (e.g. Refs. [23,27]). As a conceptual extension of the accepted behavior at grain boundaries, we propose bubble growth through vacancy absorption at line defects, i.e., dislocations, as a mechanism of intra-granular bubble coarsening. Bubbles along dislocations may absorb vacancies from the region of the medium where dislocations induce a compressive local stress state, which convoys vacancies. The condition for the activation of vacancy absorption is considered as the bubble internal energy (pressure) exceeding the mechanical equilibrium pressure. Also, as coarsened bubbles may reach a size compatible with the inter-bubble distances, bubble coalescence by impingement is also considered.

The effect of size-dependent re-solution as put forward in Refs. [24,28,38] provides an explanation for bubble coarsening that is alternative, or complementary, to the role of dislocations, and may be further investigated in the future.

In the following, we discuss modeling of the individual physical processes considered for the evolution of nanometric bubbles in the bulk and for bubble coarsening at dislocations, before presenting the formulation of the overall model in Section 3.

2.2. Bubble nucleation

Two different approaches have been proposed to model the rate of fission gas bubble nucleation in UO_2. The homogeneous mechanism describes bubble nucleation as a consequence of diffusion-limited precipitation of gas atom dimers [6,38,66], while the heterogeneous mechanism considers nucleation as a direct consequence of fission spikes [30,67,68]. Although both mechanisms are presumably active, following our previous work [30] we model the nucleation of small intra-granular bubbles in the bulk of the grain as heterogeneous. The nucleation rate ν_b ($m^{-3}s^{-1}$) is calculated as

$$\nu_b = 2\eta F \tag{1}$$

where η (bubble per fission fragment) is in the range 5–25 [19,67], F (fission $m^{-3}s^{-1}$) is the fission rate density, and the factor of 2 corresponds to the approximate number of fragments generated by each fission event.

Nucleation of bubbles lying along dislocations may be due to the precipitation of gas in the region where dislocations induce a tensile stress state, due to the larger radii of fission gas atoms with respect to U [69]. Rather than directly describing this mechanism, we choose to adopt a simplified approach. We consider a step-wise nucleation of dislocations and a subsequent constant value for simplicity, thus a one-off nucleation of associated bubbles, reading

$$\begin{aligned} N_d(t=0) &= N_{d,0} \\ \nu_d &= 0 \end{aligned} \tag{2}$$

where N_d (bubble m^{-3}) is the number density of bubbles at dislocations, $N_{d,0} = K \cdot \rho_d$, with ρ_d (m m^{-3}) being the space-averaged dislocation density in the fuel grain and K (bubble m^{-1}) a model parameter representative of the number of bubbles nucleated per dislocation, and ν_d (bubble $m^{-3}s^{-1}$) the nucleation rate of bubbles at dislocations. While this approach is followed here for simplicity, a more refined treatment is envisaged where the nucleation rate is calculated as

$$\nu_d = K \cdot \frac{d\rho_d}{dt} \tag{3}$$

and coupled to a model describing the time evolution of the dislocation density (e.g. Ref. [24]). In this work, we assume an overall representative dislocation density, without distinguishing among the different types of dislocations. Furthermore, we assume that the dislocations are immobile, i.e., we neglect conservative and non-conservative dislocation motion. The latter phenomenon is indeed playing a role at temperatures of interest for the application of the model presented here, but its inclusion in the analysis would call for a dislocation evolution model, which is beyond the scope of the present work and is left as future development.

2.3. Gas atom trapping

In the present model, we consider the trapping of single gas atoms at bubbles as well as at dislocations. In turn, gas atoms trapped at dislocations are considered to provide an additional contribution to gas inflow at bubbles that lie along dislocations. Bubbles are assumed to be spherical. Following Ham [70], the trapping rate at bubbles in the bulk is calculated as

$$\beta_b = 4\pi D R_b N_b \tag{4}$$

and the trapping rate at bubbles along dislocations is calculated as

$$\beta_d = 4\pi D R_d N_d \tag{5}$$

where β (s^{-1}) is the trapping rate, D (m^2s^{-1}) the single gas atom diffusion coefficient, R (m) the bubble radius, and N (bubble m^{-3}) the number density of bubbles, and the subscripts b and d refer to bubbles in the bulk and along dislocations, respectively. For the trapping rate at dislocations, we write

$$\beta' = \frac{2\pi D_d \rho_d}{\ln \frac{r_{ws,d}}{r_d} - \frac{3}{5}} \tag{6}$$

where β' (s^{-1}) is the trapping rate, D_d (m^2s^{-1}) is the xenon diffusivity close to the dislocation core, $r_{ws,d} = 1/\sqrt{\pi\rho_d}$ (m) the radius of the Wigner-Seitz cell associated with a dislocation, and r_d (m) is the dislocation core radius, taken equal to five times the magnitude of the UO_2 Burgers vector. The diffusion coefficient of single gas atoms in the bulk of the grain is calculated according to Turnbull and co-workers [71], whereas the gas diffusivity close to the dislocation core has been derived from the work of Murphy and co-workers [72]. The corresponding correlations are reported in a subsequent section of this work.

As a modeling assumption, gas atoms captured by dislocations are considered as instantaneously trapped into bubbles along dislocations. The hypothesis is justified by the rapid diffusion of species near the core of dislocations (pipe diffusion), as shown, e.g., by Murphy et al. [72]. In addition, direct trapping of gas atoms from the bulk at bubbles along dislocations is considered. It follows that the total rate of gas atom trapping at bubbles along dislocations is given by $\beta_d + \beta'$.

2.4. Re-solution

As for the re-solution of gas atoms from the bubbles, no clear consensus emerges from the literature regarding the dominating mechanism in uranium dioxide, i.e., whether the interaction of intra-granular bubbles with fission fragments occurs by complete bubble destruction (so-called *heterogeneous* mechanism) or by gradual re-dissolution of individual gas atoms (*homogeneous* mechanism). *Heterogeneous* re-solution was advocated by legacy theoretical works (e.g., by Turnbull [67], Blank and Matzke [73]), while the *homogeneous* mechanism was originally proposed by Nelson [74] and more recently by Schwen and coworkers [75,76]. Molecular dynamics calculations performed by Govers et al. [77] and more recently, by Setyawan et al. [78] provided support for re-solution being induced by the thermal spike due to electronic stopping, which corresponds to the heterogeneous re-solution

model, while at the same time allowing for a partial redissolution of the gas for sufficiently large bubbles, a behavior closer to the homogeneous model. In the present model, we adopt the following expression or the re-solution rate developed through molecular dynamics calculations by Setyawan et al. [78], which we apply to both bubbles in the bulk and at dislocations:

$$\alpha = \left(a\exp(-b_1 \cdot R) + \frac{b_0 - a}{1 + c \cdot R^2} \exp\left(-d \cdot R^2\right) \right) \cdot F \tag{7}$$

where α (s^{-1}) is the re-solution rate, R (m) is the bubble radius and a, b_0, b_1, c, d are parameters from Ref. [78]. In particular, we consider the parameters corresponding to a ratio between the thermal spike energy and the total electronic stopping power of 0.73, as suggested in Ref. [78]. The formulation by Setyawan et al. for the re-solution rate improves and extends through atomistic methods the legacy work on re-solution from Turnbull [67], and introduces consideration of the thermal spike energy dissipation, the off-centered ballistic distance (i.e., the distance between the thermal spike and the bubble center), and the reduced efficiency of re-solution with increasing bubble radius. The latter aspect is particularly important for the present work, where large coarsened bubbles are considered. The reduced re-solution efficiency with increasing bubble radius evaluated by Setyawan and coworkers through lower-length scale modeling confirms the theoretical conclusions fm other authors, e.g., Ref. [18,20,28].

A sketch of the processes described above is reported in Fig. 1.

2.5. Bubble coarsening along dislocations

In the proposed model, the bubble coarsening mechanism is naturally activated during transient conditions according to the physical representation adopted.

We assume that bubbles at dislocations may absorb vacancies when their internal energy (pressure) exceeds the mechanical equilibrium pressure. This condition is favored during transients to high temperatures, when additional gas atom trapping at bubbles due to enhanced thermal diffusion acts to increase bubble pressure. It is also favored for bubbles along dislocations, which undergo additional inflow of gas atoms following trapping at dislocations (Section 2.3), compared to bubbles in the bulk. As we assume that vacancies are available near dislocations, once the condition is met,

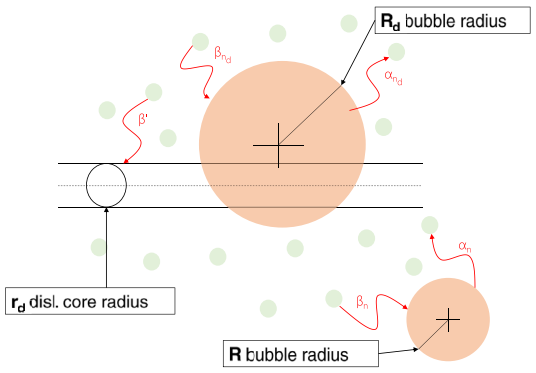

Fig. 1. Sketch of the gas atoms trapping into and re-solution from bubbles considered in the model. In particular, β_n, β_{n_d}, and β' represent the trapping of single gas atoms into bulk intra-granular bubbles, into dislocation bubbles, and on dislocation lines, respectively while α_n and α_{n_d} represent the re-solution of gas atoms from bulk and dislocation bubbles, respectively, to the matrix.

vacancy absorption at bubbles along dislocations and the associated bubble growth are considered. Modeling details are given below.

2.5.1. Vacancy absorption

The rate of vacancy absorption at a dislocation bubble is calculated using an adaptation of the Speight-Beere model [23,79–81], as

$$\frac{dn_v}{dt} = \frac{2\pi D_v \delta}{kT\zeta}\left(p - p_{eq}\right) \tag{8}$$

where n_v (vacancy $bubble^{-1}$) is the number of vacancies per bubble, D_v ($m^2 s^{-1}$) the vacancy diffusion coefficient along dislocations, δ (m) the radius of the equivalent Wigner-Seitz cell associated with a dislocation bubble,[4] k (J K^{-1}) the Boltzmann constant, T (K) the local temperature, p and p_{eq} (Pa) the bubble pressure and the equilibrium pressure, respectively, and ζ (/) a dimensionless factor calculated as [81].

$$\zeta = \frac{10\psi(1+\psi^3)}{-\psi^6 + 5\psi^2 - 9\psi + 5} \tag{9}$$

where $\psi = R_d/\delta$ is the ratio between the radii of the dislocation bubble and of the Wigner-Seitz cell. The pressure of the gas in the bubbles associated to dislocations is evaluated considering the hard sphere equation of state, in the formulation by Carnahan and Starling [82], reading

$$\frac{pV}{n_d kT} = \frac{1 + \tilde{y} + \tilde{y}^2 - \tilde{y}^3}{(1-\tilde{y})^3} \tag{10}$$

where V_d (m^3) is the bubble volume, n_d (atom $bubble^{-1}$) the number of atoms per bubble, $\tilde{y} = \pi/6(\delta_{HS}^3 \upsilon)$ (/) the packing fraction, υ (atom m^{-3}) the atomic density in the bubble, i.e., the ratio between the average number of atoms per bubble and the bubble volume, and δ_{HS} (m) the hard sphere diameter for xenon. The latter is calculated according to Brearley and MacInnes [83], considering a modified Buckingham interatomic potential and reading

$$\delta_{HS} = 4.45 \cdot 10^{-10}\left(0.8542 - 0.03996 \cdot \log\left(\frac{T}{231.2}\right)\right) \tag{11}$$

With the local temperature, T, expressed in K. The Carnahan-Starling equation of state is considered more suitable for the pressure ranges of interest in the present study, relative to other options such as the perfect gas law or the van der Waals equation of state [84,85].

The equilibrium pressure is determined by the surface energy, γ (Jm^{-2}), and the hydrostatic stress in the surrounding medium, σ_h (Pa) via the capillarity relationship, i.e.,

$$p_{eq} = \frac{2\gamma}{R_d} - \sigma_h \tag{12}$$

where p_{eq} (Pa) is the equilibrium pressure and R_d the radius of a dislocation bubble.

As for the vacancy pipe diffusion coefficient along dislocations, D_v, in the absence of available data, we consider previous work on bulk diffusivity of defects in UO_2 [86] and on pipe diffusion of interstitials [87] to derive a tentative correlation for the vacancy

[4] The radius of the Wigner-Seitz cell is determined by the relationship $4/3\pi N_d \delta^3 = 1$.

diffusivity, as follows. We apply the assumption of the ratio between the vacancy diffusion coefficients at dislocations and in the bulk being the same as for interstitial atoms, i.e.,

$$\frac{D_v}{D_{v,bulk}} = \frac{D_i}{D_{i,bulk}} \tag{13}$$

We use the bulk diffusion coefficient for vacancies and interstitials, $D_{v,bulk}$ and $D_{i,bulk}$ ($m^2 s^{-1}$), from Andersson et al. [86], and the interstitial pipe diffusion coefficient, D_i ($m^2 s^{-1}$) from the results by Murphy et al. [87]. The corresponding relations are as follows:

$$\begin{aligned} D_{v,bulk}(T) &= 7.12 \cdot 10^{-7} \exp\left(\frac{-4.72\text{eV}}{kT}\right) \\ D_{i,bulk}(T) &= 1.2 \cdot 10^{-6} \exp\left(\frac{-4.70\text{eV}}{kT}\right) \\ D_i(T) &= 6.4 \cdot 10^{-2} \exp\left(\frac{-1.82\text{eV}}{kT}\right) \end{aligned} \tag{14}$$

$$D_v.\left(m^2 s^{-1}\right) : \; D_v(T) = 3.8 \cdot 10^{-2} \exp\left(\frac{-1.84\text{eV}}{kT}\right) \tag{15}$$

The above procedure must be regarded as a tentative approach to derive an approximate correlation for vacancy diffusivity in the dislocation core. More refined analyses that better characterize this parameter are of interest as a future development. Indeed, it can be noticed how the derived activation energy is compatible with the analysis by Murphy and co-authors, reported in Refs. [87]. The diffusion coefficients in Eqs. (14) and (15) are plotted in Fig. 2.

2.5.2. Bubble coalescence

As the radius of coarsened bubbles at dislocations can become comparable with the average inter-bubble distance [11,14], interconnection of bubbles and the associated bubble coalescence need to be considered. Following [88], we consider intra-granular bubbles as a three-dimensional system of spheres, randomly distributed according to a Poisson distribution. Torquato [89] showed that inter-connection occurs when bubbles are sufficiently large and high in number, i.e., when their volume fraction (i.e., porosity) is sufficiently high, around 10%. This value is consistent with experimental SEM observations of intra-granular coarsened bubbles [11,14], supporting the inclusion of a bubble interconnection description in the present model.

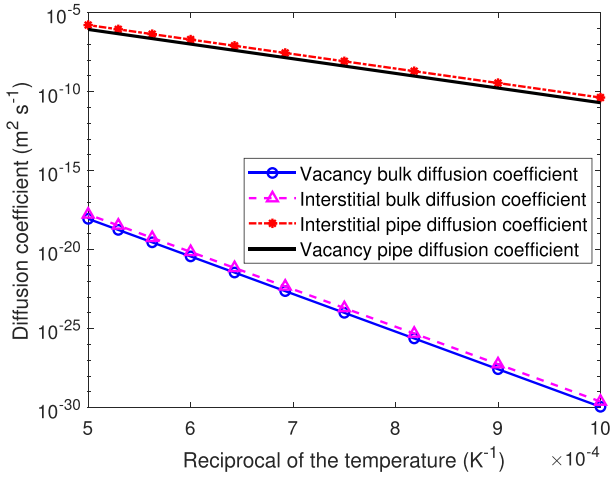

Fig. 2. Adopted correlations for the diffusion coefficients of vacancies and interstitials in UO_2 as a function of the temperature.

For the system of two populations of intra-granular bubbles considered in this work, i.e., one in the bulk of the grain and one associated with dislocations, two modes of inter-connection are modeled. In particular, we neglect coalescence between nanometric bulk bubbles, and account for coalescence between (i) two large bubbles along dislocations and (ii) one dislocation bubble and one bulk bubble.

The inter-connection between two large dislocation bubbles is modeled assuming that only pair interactions take place and considering bubbles as hard-spheres. The first assumption is made to overcome the need of knowing the non-trivial complete probability density function for a system of hard-spheres, which is replaced by the nearest-neighbor distribution function. The second assumption avoids the nonphysical possibility for two intra-granular bubbles to share the same region of a fuel grain. Following the work done in Ref. [90], the equation for the variation rate of the number density of dislocation bubbles due to coalescence can be obtained from Ref. [89] as

$$\frac{dN_d}{N_d} = -\frac{1}{2} \int_1^{1+\frac{dR_d}{R_d}} H(x)dx \tag{16}$$

where $x = r/2R_d$ is the normalized distance between two dislocation bubbles, N_d the dislocation bubble number density, and $H(x)$ is the nearest-neighbor distribution function for hard-spheres [89,91,92]. Equation (16) is reshaped as follows

$$\frac{dN_d}{dV_d} = -4\lambda N_d^2 \tag{17}$$

where V_d (m) is the bubble volume, and $\lambda = (2-\xi)/[2(1-\xi)^3]$ is a correction factor accounting for the hard-sphere assumption, with $\xi = \frac{4}{3}\pi R_d^3 N_d$ being the porosity associated with dislocation bubbles. As a consequence of coalescence, the number density of dislocation bubbles decreases while the total gas content remains the same, which corresponds to a higher number of gas atoms per bubble and consequently, an increased average radius. It must be noticed that the current formulation of the interconnection model may need further investigation to estimate the impact of the array disposition of bubbles attached to dislocations, which may increase the probability of interaction [89].

As for the interaction between a dislocation bubble and a bulk bubble,[5] we assume that all the bulk bubbles which belong to a sphere of volume $V_d^* = \frac{4}{3}\pi(R_d + R)^3$ are captured by the expanding dislocation bubble, transferring all their gas content to the latter. The probability that a small bubble is incorporated by a growing dislocation bubble is $N_b \cdot dV_d^*$, with $dV_d^* = 4\pi(R_d + R)^2 dR_d$. Consequently, the decrease in number density of bulk bubbles due to coalescence with dislocation bubbles is given by

$$\frac{dN_b}{dV_d^*} = -N_d \cdot N_b \tag{18}$$

[5] The present model does not account for bulk bubble mobility in isothermal conditions, since we focus on in-pile transients. Although experimentally observed to some extent [39], no clear consensus arises in the literature about it [48,93]. A possible way of including bubble mobility in the present modeling framework is presented in Ref. [94].

3. Model formulation

Considering the mechanisms described in Section 2, the developed model of intra-granular bubble evolution extends the normal operating conditions model developed in Ref. [30] by adding consideration of a second population of bubbles along dislocations, wubject to coarsening driven by vacancy absorption. Moreover, in line with the formulation of the re-solution parameter proposed by Setyawan and coauthors [78], we consider a gradual (*homogeneous*) re-solution of atoms from bubbles as opposed to complete bubble destruction in a re-solution event, similar to the treatment proposed in Ref. [81]. While both small bubbles in the bulk and coarsening bubbles at dislocations are modeled, only the average size of each population is considered.

The system of coupled partial differential equations governing the evolution of fission gas atom concentrations is

$$\begin{cases} \dfrac{\partial c}{\partial t} = D\nabla^2 c - (\beta_b + \beta_d + \beta')c + \alpha_b\phi_b m_b + \alpha_d\phi_d m_d - 2(\nu_b + \nu_d) + yF \\ \dfrac{\partial m_b}{\partial t} = 2\nu_b + \beta_b c - \alpha_b\phi_b m_b \\ \dfrac{\partial m_d}{\partial t} = 2\nu_d + (\beta_d + \beta')c - \alpha_d\phi_d m_d \end{cases} \tag{19}$$

where c (atom m^{-3}) is the concentration of single gas atoms, m_b (atom m^{-3}) the total concentration of gas in bulk bubbles, m_d (atom m^{-3}) the total concentration of gas in dislocation bubbles, and y (atom fission^{-1}) the fission yield. The coefficients are defined in Section 2, with the subscript b and d distinguishing between the parameters referring to bulk and dislocation bubbles, respectively. The evolution of bubble number densities is governed by

$$\begin{aligned} \frac{\partial N_b}{\partial t} &= \nu_b - \alpha_n\phi_b N_b - N_d \cdot N_b \frac{\partial V_d}{\partial t} \\ \frac{\partial N_d}{\partial t} &= \nu_d - \alpha_{n_d}\phi_d N_d - 4\lambda N_d^2 \frac{\partial V_d}{\partial t} \end{aligned} \tag{20}$$

where the first term corresponds to nucleation, the second to re-solution and the third to coalescence. As mentioned in Section 2, we consider a one-off nucleation of dislocations and associated bubbles, whose initial value is given by the product of the dislocation density times the model parameter K (Eq. (2)). The average number of gas atoms per bubble for bulk and dislocation bubbles, respectively, is given by

$$\begin{aligned} n_b &= \frac{m_b}{N_b} \\ n_d &= \frac{m_d}{N_d} \end{aligned} \tag{21}$$

Following [81], the corrections of the re-solution rates accounting for one-by-one re-solution of atoms in the homogeneous mechanism – namely, ϕ_b and ϕ_d – are calculated as

$$\begin{aligned} \phi_b &= \frac{1}{n_b - 1} \\ \phi_d &= \frac{1}{n_d - 1} \end{aligned} \tag{22}$$

Solution of Eqs. (19)–(21) provides the number densities and average numbers of atoms per bubble of the two populations. As discussed in Section 2.5, dislocation bubbles are considered to absorb vacancies from the compressive-stress region next to the dislocation core when their internal energy exceeds the equilibrium value, while this relaxation mechanism is not considered for bulk bubbles (vacancy starvation [46,49,50]). The volume of dislocation bubbles (assumed to be spherical) is determined by their gas atom and vacancy contents according to the following relationship

$$V_d = n_d\omega + n_v\Omega \tag{23}$$

where ω (m^3atom^{-1}) is the volume of a fission gas atom, calculated consistently with the adopted equation of state,[6] and Ω (m^3vacancy^{-1}) is the vacancy volume. The volume of bulk bubbles (also assumed spherical) is calculated as (e.g. Ref. [6,30])

$$V_b = n_b B \tag{24}$$

where B (m^3) is the volume occupied by a fission gas atom in an intra-granular bubble. Finally, the fractional increment in fuel volume, V_f (m^3), due to intra-granular gaseous swelling[7] is computed as

$$\frac{\Delta V_f}{V_f} = N_d V_d + N_b V_b \tag{25}$$

The formulation of the model calls for further considerations on the underlying assumptions. First, the evolution of the dislocation density under irradiation is not modeled in this work. Rather, we consider a constant value, not dependent on temperature and/or burnup. However, Nogita and Une [96] found an exponential dependence of the dislocation density on the local burnup, analyzing the rim zone of light water reactor UO_2 fuel (i.e., where temperatures are relatively low throughout the irradiation). These experimental findings need to be considered if the present model is applied to high burnup conditions. It is worth noting that the inclusion of dislocation evolution in fission gas behavior modeling is very challenging. In particular, the attempt of describing the evolution of dislocations under irradiation requires detailed modeling of point and extended defect evolution (e.g. Refs. [97–100]). Such models account for dislocation evolution in a mechanistic fashion, yet they are featured by a complexity level which may not be compatible with requirements of engineering fuel performance codes. While modeling dislocation evolution (especially accounting for the non-conservative motion at high temperatures) is of interest in perspective, it is out of the scope of the present work.

Considering a constant value for the dislocation density along with the simplified model for nucleation (Eq. (2)) results in a "one-off" nucleation of dislocation bubbles, whose number density may then evolve due to irradiation-induced re-solution and interconnection. Although this is a significant simplification, we choose not to model explicitly nucleation of bubbles along dislocations to avoid the introduction of further model parameters which may be affected by high uncertainties.

The new model generalizes the description of the intra-granular behavior of fission gas bubbles already presented in Ref. [30], extending it to the evolution of dislocation bubbles and the coarsening phenomenon. While preserving a physical foundation, the final model formulation entails a limited number of equations and parameters, which makes it suitable for incorporation in engineering-scale fuel performance codes.

[6] We assume that fission gas atoms diffuse via neutral complexes of defects (Schottky trios, i.e., one vacancy from the uranium sublattice and two vacancies from the oxygen sublattice [95]). Thus, when captured into a bubble, atoms bring about a contribution to the bubble volume.

[7] It must be noted that the swelling we are referring to does not consider the contribution of fission products dissolved in the fuel matrix.

Table 1
Nomenclature and corresponding values or correlations for the characteristic rates and parameters of the intra-granular bubble evolution model.

Symbol	Definition	Value	U·O.M.	Reference
a	Re-solution model parameter	$9.49 \cdot 10^{-24}$	m^3	[78]
b_1	Re-solution model parameter	$7.07 \cdot 10^{-2}$	m^{-1}	[78]
b_0	Re-solution model parameter	$9.18 \cdot 10^{-23}$	m^3	[78]
c	Re-solution model parameter	7.982	m^{-2}	[78]
d	Re-solution model parameter	$3.71 \cdot 10^{-2}$	m^{-2}	[78]
K	Number of bubbles nucleated per dislocation	$1 \cdot 10^6$	bubble m^{-1}.	Present work
B	Volume occupied by a fission gas atom in intra-granular bubbles	$4.09 \cdot 10^{-29}$	m^3	[6,30,102]
D	Diffusion coefficient of fission gas atoms in UO_2 $D = D_1 + D_2 + D_3$ $D_1 = 7.6 \cdot 10^{-10} \exp(-4.86 \cdot 10^{-19}/kT)$ $D_2 = 5.64 \cdot 10^{-25} \sqrt{\dot{F}} \exp(-1.91 \cdot 10^{-19}/kT)$ $D_3 = 2 \cdot 10^{-40} F$		$m^2 s^{-1}$	[71]
D_d	Diffusion coefficient of xenon close to the dislocation core $D_d = 7.74 \cdot 10^{-6} \exp(-1.21 \cdot 10^{-19}/kT)$		$m^2 s^{-1}$	[72]
b	UO_2 Burgers vector magnitude	$3.85 \cdot 10^{-10}$.	m	–
r_d	Dislocation core radius	$5 \cdot b$	m	E.g. [59],
γ	UO_2 gas surface energy	0.7	$Jm-2$	E.g. [5],
η	Number of bubbles nucleated per fission fragment	25	bubble per fission fragment	[5]
ρ_d	Average dislocation density in the fuel grain	$4 \cdot 10^{13}$	mm^{-3}	E.g. [14],
Ω	Vacancy co-volume	$4.09 \cdot 10^{-29}$	m^3 vacancy^{-1}	[102]

4. Model comparisons to experimental data

In this Section, we present the comparisons of model predictions to experimental data. The nominal values of the parameters used in the model are summarized in Table 1. We implemented the presented model in, and performed the simulations through, the SCIANTIX code [93], a stand-alone, meso-scale computer code developed at Politecnico di Milano, aimed at simulating fission gas behavior in nuclear fuels. It constitutes a flexible tool for the development, verification, and validation of mechanistic fission gas behavior models.

4.1. Experimental database

The database chosen to validate the model is the SEM experimental database by White and coworkers [14]. The database consists in measurements performed on 12 UO_2 Advanced Gas Reactor samples of fuel rods irradiated up to burnup between 9 and 21 $GWdt^{-1}$ in the Halden reactor. After the base irradiation, rods were subjected to power ramp or power cycle histories. SEM examinations were then performed at different radial positions, obtaining from 3 to 7 radial examinations on each sample. The obtained measurements compose a wide database of local measurements for

Table 2
Details about burnup, power histories and SEM analyses of the fuel samples of the considered SEM database [14].

Rod ID	Burnup ($GWdt^{-1}$)	Ramp type	Peak power (kWm^{-1})	Hold time	SEM radial points
4000	20.7	Fast	40.0	30.0 min	4
4004	20.5	Fast	40.0	2.38 min	4
4005	20.8	Fast	40.0	2 min	4
4064	20.1	Slow	43.0	–	4
4065	9.25	Slow	41.8	–	5
4135	15	Slow + Fast	36.9	80 s	3
4136	12	Slow + Fast	39.0	–	5
4140	12	Slow	36.0	–	3
4162	12.6	Slow	40.0	–	4
4163	12.6	Fast	35.0	2.0 min	4

Table 3
Detailed description of the power histories performed on the fuel samples of the considered SEM database [14].

Rod ID	P_1 (kWm^{-1})	τ_1	τ_{2a} (min)	P_2 (kWm^{-1})	τ_{2b} (min)	τ_{2c}	P_3 (kWm^{-1})	τ_3	τ_4
4000	14.0	12 d	1.52	40.0	30.0	100 s	14.0	99.0 min	SCRAM
4004	14.0	12 d	1.97	40.0	2.38	90 s	14.0	99.0 min	SCRAM
4005	14.0	12 d	1.32	40.0	2.0	–	SCRAM	–	–
4064	20.0	15 wk	47.0	43.0	0.0	–	SCRAM	–	–
4065	19.3	3 wk	47.0	41.8	0.0	–	SCRAM	–	–
4135	18.5	1 wk	65.0	36.9	0.0	40 s			
	13.0	8.0 min	40 s	36.9	80 s	40 s			
	13.0	0.0	40 s	36.9	80 s	40 s	16.0	28 d	6 h
4136	16.5	1 wk	63.0	36.0	0.0	–			
	36.0	0.0	2.0	39.0	0.0	40 s	16.0	27 d	6 h
4140	16.5	1 wk	65.0	36.0	0.0	40 s	16.0	27 d	6 h
4162	18.0	3 wk	45.0	40.0	0.0	40 s	18.0	6 min	–
4163	18.0	3 wk	45.0	35.0	0.0	40 s	18.0	41 h	–

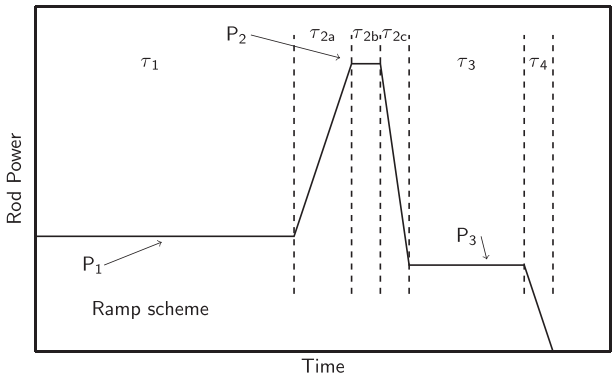

Fig. 3. Schematic representation of a generic ramp test from the considered experiments [14]. For the meaning of the symbols, the reader is referred to Table 3.

sizes and number densities of intra-granular bubbles, and of intra-granular swelling. Details about the irradiation conditions are given in Tables 2 and 3, and a sketch of power ramps is provided in Fig. 3. The specific power, temperature, and hydrostatic stress for each SEM sample, needed as inputs for SCIANTIX simulations, are calculated values from the ENIGMA code [101]. The experimental data considered in this work in terms of intra-granular bubble radius, density, and resulting swelling refers to the second peak of the observed, bi-modal intra-granular bubble size distribution as compiled by White and coworkers [14], which is deemed to be associated to dislocation bubbles.

4.2. Results

The comparisons of simulations to experimental data from Ref. [14] are reported in Figs. 4–6 for the average bubble radius (Fig. 4), number density (Fig. 5), and corresponding gaseous swelling (Fig. 6). Experimental data and simulation results for both quantities are collected in Table 4. For comparison, we include also the results obtained applying the model by Pizzocri et al. [30] (black symbols in Figs. 4–6). It must be underlined that the model by Pizzocri and coworkers does not feature a description of bubble coarsening. Its inclusion is rather intended as to demonstrate how

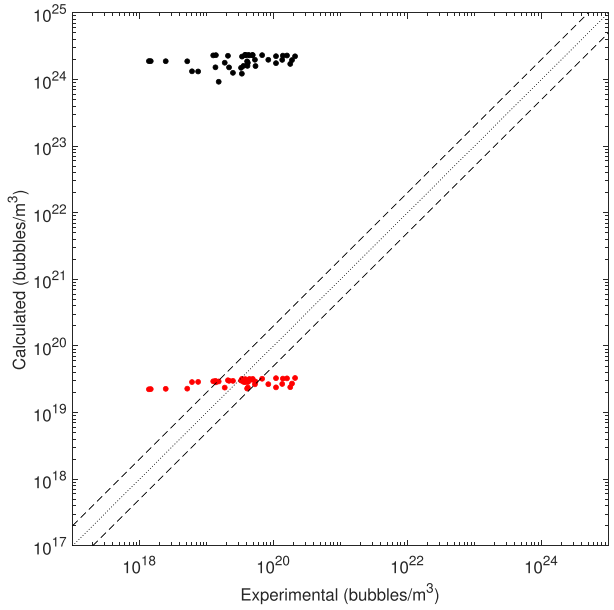

Fig. 5. Comparisons of model predictions for bubble number density to experimental data from Ref. [14]. Each symbol corresponds to a local simulation for one of the SEM radial points in the experimental database. Both results obtained with the new transient model (red symbols) and with the previous normal operation model [30] (black symbols) are included. (For interpretation of the references to colour in this figure legend, the reader is referred to the Web version of this article.)

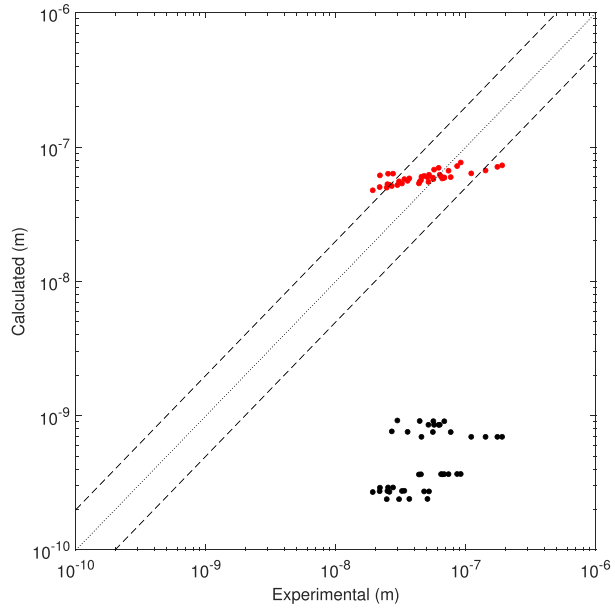

Fig. 4. Comparisons of model predictions for bubble radius to experimental data from Ref. [14]. Each symbol corresponds to a local simulation for one of the SEM radial points in the experimental database. Both results obtained with the new transient model (red symbols) and with the previous normal operation model [30] (black symbols) are included. (For interpretation of the references to colour in this figure legend, the reader is referred to the Web version of this article.)

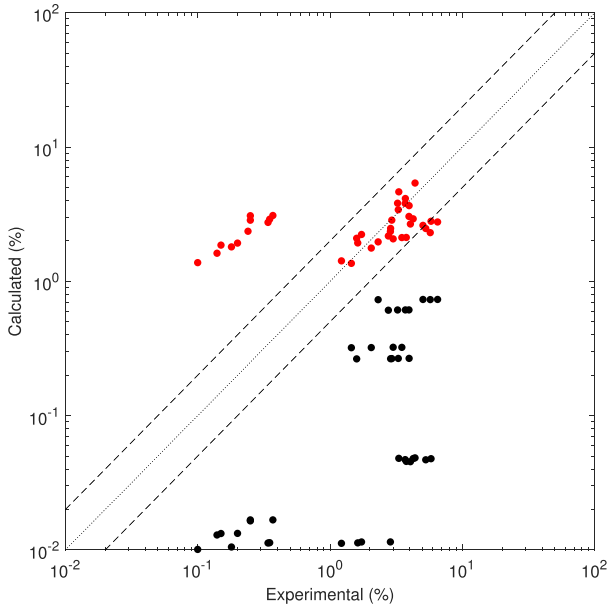

Fig. 6. Comparisons of model predictions for bubble swelling to experimental data from Ref. [14]. Each symbol corresponds to a local simulation for one of the SEM radial points in the experimental database. Both results obtained with the new transient model (red symbols) and with the previous normal operation model [30] (black symbols) are included. (For interpretation of the references to colour in this figure legend, the reader is referred to the Web version of this article.)

Table 4
Comparison of calculated intra-granular bubble radius and gaseous swelling to experimental data for the analyzed fuel samples from Ref. [14]. A total of 40 sample locations is considered in the present work.

Sample ID	Bubble radius (nm)		Bubble density $\times 10^{-19}$ (bubble m^{-3})		Gaseous swelling (%)	
	Experimental [14]	Calculated	Experimental [14]	Calculated	Experimental [14]	Calculated
4000–A	91.2	77.0	1.38	2.79	4.39	5.35
4000–B	85.6	72.1	1.26	2.90	3.31	4.54
4000–C	73.5	65.9	2.09	3.02	3.7	3.62
4000–D	65.8	55.3	3.39	3.19	4.05	2.27
4004–A	64.4	57.6	3.80	3.16	4.25	2.54
4004–B	68.1	56.4	4.38	3.18	5.8	2.39
4004–C	45.1	52.5	13.8	3.24	5.29	1.96
4004–D	43.5	46.8	10.9	3.31	3.77	1.42
4005–A	68.2	56.2	4.90	3.19	6.5	2.37
4005–B	56.2	54.4	6.77	3.22	5.04	2.17
4005–C	44.1	50.2	15.9	3.27	5.72	1.74
4005–D	29.7	43.4	21.0	3.35	2.31	1.15
4064–A	61.7	73.7	3.77	2.64	3.71	4.43
4064–B	56.9	71.5	4.20	2.68	3.24	4.10
4064–C	62.9	65.4	3.78	2.77	3.95	3.25
4064–D	51.5	55.9	4.82	2.90	2.76	2.12
4065–A	189.9	80.4	0.14	1.77	3.96	3.86
4065–B	174.6	78.6	0.15	1.78	3.28	3.61
4065–C	141.6	74.3	0.25	1.78	2.93	3.05
4065–D	109.9	71.2	0.52	1.77	2.87	2.67
4065–E	45.5	67.7	4.04	1.76	1.59	2.28
4135–A	27.5	67.2	4.09	2.54	0.37	3.22
4135–B	25.2	67.1	3.57	2.54	0.25	3.21
4135–C	21.8	65.1	5.39	2.56	0.25	2.96
4136–A	52	68.4	0.61	2.34	0.35	3.13
4136–B	47.7	67.0	0.75	2.35	0.34	2.96
4136–C	33.6	63.3	1.52	2.37	0.24	2.52
4136–D	25.8	56.4	2.48	2.40	0.18	1.81
4136–E	19.2	48.7	3.37	2.42	0.10	1.17
4140–A	32.2	59.9	1.36	2.44	0.20	2.19
4140–B	24.9	59.0	2.17	2.44	0.15	2.10
4140–C	21.7	55.6	3.28	2.45	0.14	1.76
4162–A	50.6	65.8	5.28	2.09	2.86	2.49
4162–B	36.7	64.7	8.37	2.09	1.73	2.37
4162–C	30.6	61.6	13.5	2.09	1.62	2.04
4162–D	24.6	55.1	18.9	2.06	1.22	1.44
4163–A	76.4	69.3	1.87	1.47	3.49	2.06
4163–B	55.7	68.9	4.14	1.47	3.0	2.01
4163–C	35.6	65.3	10.9	1.44	2.05	1.68
4163–D	26.9	58.9	17.8	1.42	1.45	1.21

the previous model is not able to represent the gaseous swelling due to coarsened bubbles, thus to highlight the added value brought about by the model we are proposing.

The overall agreement between experimental data and model predictions (red symbols in Figs. 4–6) appears satisfactory for this initial application. In particular, sizes of tens to hundreds of nanometers for the coarsened intra-granular bubbles, and volumetric swellings of one to several percent, in these ramp-tested fuel samples are reproduced. Note that these values are orders of magnitude higher than bubbles sizes and swellings observed under normal operating conditions, and could not be captured with traditional models that do not include specific transient capabilities. This is confirmed by the comparison with the results obtained using the previous model (black symbols).

Calculations with the present model exhibit deviations of calculated bubble radii from the experimental data smaller than a factor of 2 for the majority of cases. As for the bubble number densities, the agreement with the experimental data is less satisfactory. This suggests that improvements may be needed in particular for the description of bubble nucleation along dislocations. Indeed, the model from Ref. [30] yields higher deviations from the experimental data. For gaseous swelling, indeed, appreciable deviations associated with the new model are found, predominately on a subset of samples (labeled 4135 and 4136), which are featured by the smallest swelling values in the considered database. It is worth noting that White and coworkers commented these lower values of gaseous swelling as unexpected, however, no justification for these observations was provided.

Fig. 7 illustrates results specific to a case chosen among those analyzed in this work, i.e. sample 4005–A. The evolution of bubble pressure during the ramp test is shown in Fig. 7a: the initial rise due to the temperature increase triggers vacancy absorption, which in turn results in bubble volume increase. The volume increase associated with vacancy absorption leads to bubble pressure relaxation, as it is demonstrated by the evolution of bubble internal pressure. In Fig. 7b, bubble coarsening is appreciable in the radius increase, which is a consequence of vacancy absorption and bubble coalescence. Gaseous swelling increases correspondingly.

5. Conclusions

In this work, we presented a model describing intra-granular fission gas behavior in UO_2 that accounts for the bubble coarsening phenomenon under in-pile, high temperature transient conditions, and the corresponding contribution to gaseous fuel swelling. In particular, the model considers the role of dislocations as a source of vacancies and preferential growth along dislocations as the mechanism for bubble coarsening in the fuel grains. This theory finds support in the experimental observations showing coarsened bubbles associated with dislocations [9,10,14,19]. It also

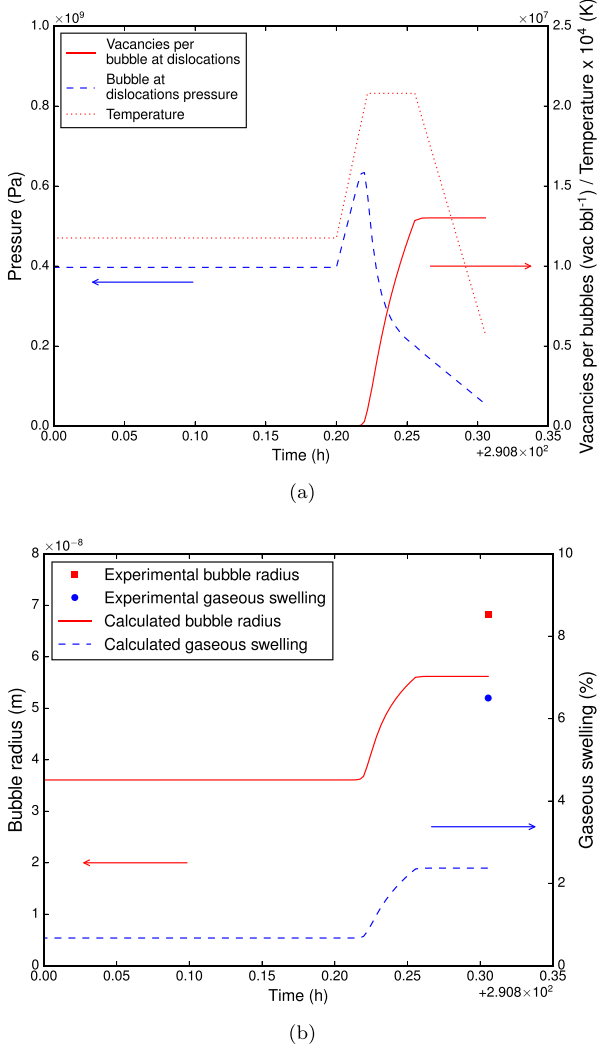

Fig. 7. Predictions for the evolution of dislocation bubble pressure and number of vacancies (a), radius and associated gaseous swelling (b) during the ramp test for the simulation of the sample 4005−A from Ref. [14].

appears to be a straightforward conceptual extension to dislocation defects of the established behavior at grain boundary bubbles.

The model extends a previous work published by the authors [30] on intra-granular bubble evolution under normal operating conditions. A multiscale approach was adopted in that the model is informed with parameters derived through atomistic calculations for irradiation-induced re-solution and defect diffusivities. The model combines a physically-sound description of bubble evolution to a limited complexity and is intended for application in engineering fuel performance codes.

The stand-alone model was applied to simulations of local fission gas behavior for the experimental database by White and coworkers. Comparisons to experimental data showed an overall satisfactory agreement between calculated values and experimental data in terms of both bubble radius and associated gaseous swelling, while comparisons in terms of bubble number density were less satisfactory. In particular, sizes of tens to hundreds of nanometers for the coarsened intra-granular bubbles, and volumetric swellings of one to several percent, in these ramp-tested fuel samples were reproduced. These values are orders of magnitude higher than bubbles sizes and swellings observed under normal operating conditions, and could not be captured with traditional models that do not include specific transient capabilities.

The model has been implemented into Idaho National Laboratory's fuel performance code BISON and is going to be made available to TRANSURANUS via its coupling with SCIANTIX. Model application to the simulation of other experimental conditions for which bubble coarsening has been observed, such as post-irradiation annealing and high burnup, is left to future work. Future work will also include the application of the model to integral fuel rod thermo-mechanics simulations. Model comparisons to detailed cluster dynamics simulations is also of interest in perspective. Moreover, future improvements may include the coupling to a model for dislocation density evolution under irradiation, and the development of a more detailed model of bubble nucleation at dislocations. Finally, the physics-based approach to the description of intra-granular gas behavior considered in the present model may be applied to other types of oxide fuels, such as plutonium-uranium mixed oxide (MOX) fuels both in light water or fast reactor conditions, provided that model parameters are updated to comply with the specific material and reactor peculiarities.

Declaration of competing interest

The authors declare that they have no known competing financial interests or personal relationships that could have appeared to influence the work reported in this paper.

CRediT authorship contribution statement

T. Barani: Conceptualization, Methodology, Software, Validation, Writing - original draft, Writing - review & editing, Visualization. **G. Pastore:** Conceptualization, Methodology, Software, Validation, Writing - original draft, Writing - review & editing, Visualization, Supervision, Funding acquisition. **A. Magni:** Methodology, Software, Validation, Writing - original draft, Writing - review & editing, Visualization. **D. Pizzocri:** Conceptualization, Methodology, Software, Validation, Writing - original draft, Writing - review & editing. **P. Van Uffelen:** Writing - original draft, Writing - review & editing, Supervision. **L. Luzzi:** Writing - original draft, Writing - review & editing, Funding acquisition, Supervision.

Acknowledgments

This research has received funding from the U.S. Department of Energy, Office of Nuclear Energy through the Scientific Discovery through Advanced Computing (SciDAC) project on Simulation of Fission Gas. The work contributes to the U.S.-EURATOM International Nuclear Energy Research Initiative (INERI) project 2017-004-E on Modelling of Fission Gas Behaviour in Uranium Oxide Nuclear Fuel Applied to Engineering Fuel Performance Codes.

This work has received funding from the Euratom research and training programme 2014−2018 through the INSPYRE Project under grant agreement No. 754329, and contributes to the Joint Programme on Nuclear Materials (JPNM) of the European Energy Alliance (EERA), in the specific framework of the COMBATFUEL Project.

The submitted manuscript has been authored by a contractor of the U.S. Government under Contract DE-AC07-05ID14517. Accordingly, the U.S. Government retains a non-exclusive, royalty free license to publish or reproduce the published form of this contribution, or allow others to do so, for U.S. Government purposes.

Appendix A. Supplementary data

Supplementary data to this article can be found online at https://doi.org/10.1016/j.jnucmat.2020.152195.

References

[1] D.R. Olander, Fundamental Aspects of Nuclear Reactor Fuel Elements Fundamental Aspects of Nuclear Reactor Fuel Elements, 1976, https://doi.org/10.1016/0022-3115(77)90226-4.

[2] P. Van Uffelen, J. Hales, W. Li, G. Rossiter, R. Williamson, A review of fuel performance modelling, J. Nucl. Mater. 516 (2019) 373–412, https://doi.org/10.1016/j.jnucmat.2018.12.037.

[3] H. Matzke, Gas release mechanisms in UO_2 - a critical review, Radiat. Eff. 53 (1980) 219–242.

[4] C. Ronchi, Physical processes and mechanisms related to fission gas swelling in MX-type nuclear fuels, J. Nucl. Mater. 84 (1–2) (1979) 55–84, https://doi.org/10.1016/0022-3115(79)90150-8.

[5] R.J. White, M.O. Tucker, A new fission gas release model, J. Nucl. Mater. 118 (1) (1983) 1–38.

[6] D.R. Olander, D. Wongsawaeng, Re-solution of fission gas - a review: Part I. Intragranular bubbles, J. Nucl. Mater. 354 (1–3) (2006) 94–109, https://doi.org/10.1016/j.jnucmat.2006.03.010.

[7] M. Tonks, D. Andersson, R. Devanathan, R. Dubourg, A. El-Azab, M. Freyss, F. Iglesias, K. Kulacsy, G. Pastore, S.R. Phillpot, M. Welland, Unit mechanisms of fission gas release: current understanding and future needs, J. Nucl. Mater. 504 (2018) 300–317.

[8] J. Rest, M. Cooper, J. Spino, J. Turnbull, P. Van Uffelen, C. Walker, Fission gas release from UO_2 nuclear fuel: a review, J. Nucl. Mater. 513 (2019) 310–345, https://doi.org/10.1016/J.JNUCMAT.2018.08.019.

[9] J. Killeen, C. Baker, Fission gas release during post irradiation annealing of UO_2 up to 1750°C, in: Proceedings of the ANS Topical Meeting on LWR Fuel Performance, ANS, Orlando, Florida, 1985.

[10] G.J. Small, Bubble development and fission gas release during rapid heating of 18 GWd/TeU UO_2, in: Specialists Meeting of Fission Product Release and Transport in Gas-Cooled Reactors, 1985, pp. 114–137. Berkeley, UK.

[11] S. Kashibe, K. Une, K. Nogita, Formation and growth of intragranular fission gas bubbles in UO_2 fuels with burnup of 6-83 GWd/t, J. Nucl. Mater. 206 (1993) 22–34.

[12] I. Zacharie, S. Lansiart, P. Combette, M. Trotabas, M. Coster, M. Groos, Thermal treatment of uranium oxide irradiated in pressurized water reactor: swelling and release of fission gases, J. Nucl. Mater. 255 (2–3) (1998) 85–91.

[13] R.J. White, The growth of intra-granular bubbles in post-irradiation annealed UO_2 fuel, in: Technical Committee Meeting on Nuclear Fuel Behaviour Modelling at High Burnup and its Experimental Support, IAEA, Windermere, UK, 2000, pp. 91–104.

[14] R.J. White, R.C. Corcoran, P.J. Barnes, A summary of swelling data obtained from the AGR/halden ramp test programme, Tech. Rep. R&T/NG/EXT/REP/0206/02 (2006).

[15] P. Losonen, On the behaviour of intragranular fission gas in UO_2 fuel, J. Nucl. Mater. 280 (1) (2000) 56–72, https://doi.org/10.1016/S0022-3115(00)00028-3.

[16] M. Mogensen, C. Walker, I. Ray, M. Coquerelle, Local fission gas release and swelling in water reactor fuel during slow power transients, J. Nucl. Mater. 131 (1985) 162–171, https://doi.org/10.1016/S0065-2881(08)60234-5.1310.1707v3.

[17] P. Garcia, G. Martin, C. Sabathier, G. Carlot, A. Michel, P. Martin, B. Dorado, M. Freyss, M. Bertolus, R. Skorek, J. Noirot, L. Noirot, O. Kaitasov, S. Maillard, Nucleation and growth of intragranular defect and insoluble atom clusters in nuclear oxide fuels, Nucl. Instrum. Methods Phys. Res. Sect. B Beam Interact. Mater. Atoms 277 (2012) 98–108, https://doi.org/10.1016/j.nimb.2011.12.031.

[18] P. Losonen, On the effect of irradiation-induced resolution in modelling fission gas release in UO_2 LWR fuel, J. Nucl. Mater. 496 (2017) 140–156, https://doi.org/10.1016/j.jnucmat.2017.09.015.

[19] C. Baker, The fission gas bubble distribution in uranium dioxide from high temperature irradiated SGHWR fuel pins, J. Nucl. Mater. 66 (1977) 283–291.

[20] J. Rest, A. Zawadski, FASTGRASS : A Mechanistic Model for the Prediction of Xe, I, Cs, Te, Ba, and Sr Release from Nuclear Fuel under Normal and Severe-Accident Conditions, 1993. Report NUREG/CR-5840.

[21] P. Lösönen, Modelling intragranular fission gas release in irradiation of sintered LWR UO_2 fuel, J. Nucl. Mater. 304 (1) (2002) 29–49.

[22] P. Van Uffelen, Contribution to the Modelling of Fission Gas Release in Light Water Reactor Fuel, Université de Liège, 2002. Ph.D. thesis.

[23] R.J. White, The development of grain-face porosity in irradiated oxide fuel, J. Nucl. Mater. 325 (1) (2004) 61–77, https://doi.org/10.1016/j.jnucmat.2003.10.008.

[24] M.S. Veshchunov, V.D. Ozrin, V.E. Shestak, V.I. Tarasov, R. Dubourg, G. Nicaise, Development of the mechanistic code MFPR for modelling fission-product release from irradiated UO_2 fuel, Nucl. Eng. Des. 236 (2) (2006) 179–200, https://doi.org/10.1016/j.nucengdes.2005.08.006.

[25] J.A. Turnbull, C.E. Beyer, Background and Derivation of ANS-5.4 Standard Fission Product Release Model, Tech. Rep, United States Nuclear Regulatory Commission, 2010.

[26] L. Noirot, MARGARET: a comprehensive code for the description of fission gas behavior, Nucl. Eng. Des. 241 (6) (2011) 2099–2118, https://doi.org/10.1016/j.nucengdes.2011.03.044.

[27] G. Pastore, L. Luzzi, V. Di Marcello, P. Van Uffelen, Physics-based modelling of fission gas swelling and release in UO_2 applied to integral fuel rod analysis, Nucl. Eng. Des. 256 (2013) 75–86, https://doi.org/10.1016/j.nucengdes.2012.12.002.

[28] M.S. Veshchunov, V.I. Tarasov, Modelling of irradiated UO_2 fuel behaviour under transient conditions, J. Nucl. Mater. 437 (1–3) (2013) 250–260, https://doi.org/10.1016/j.jnucmat.2013.02.011.

[29] G. Jomard, C. Struzik, A. Boulore, P. Mailhé, V. Auret, R. Largenton, Caracas : an industrial model for the description of fission gas behavior in LWR-UO_2 fuel, in: World Reactor Fuel Performance Meeting, vol. 100154, 2014, pp. 14–17. Sendai, Japan.

[30] D. Pizzocri, G. Pastore, T. Barani, A. Magni, L. Luzzi, P.V. Uffelen, S.A. Pitts, A. Alfonsi, J.D. Hales, A model describing intra-granular fission gas behaviour in oxide fuel for advanced engineering tools, J. Nucl. Mater. 502 (2018) 323–330.

[31] M.H.A. Piro, D. Sunderland, S. Livingstone, J. Sercombe, W. Revie, A. Quastel, K.A. Terrani, C. Judge, A review of pellet–clad interaction behavior in zirconium alloy fuel cladding. Reference Module in Materials Science and Materials Engineering, Elsevier, 2017.

[32] G. Pastore, L.P. Swiler, J.D. Hales, S.R. Novascone, D.M. Perez, B.W. Spencer, L. Luzzi, P. Van Uffelen, R.L. Williamson, Uncertainty and sensitivity analysis of fission gas behavior in engineering-scale fuel modeling, J. Nucl. Mater. 456 (2015) 398–408, https://doi.org/10.1016/j.jnucmat.2014.09.077.

[33] T. Barani, E. Bruschi, D. Pizzocri, G. Pastore, P. Van Uffelen, R.L. Williamson, L. Luzzi, Analysis of transient fission gas behaviour in oxide fuel using BISON and TRANSURANUS, J. Nucl. Mater. 486 (2017) 96–110, https://doi.org/10.1016/j.jnucmat.2016.10.051.

[34] K. Lassmann, TRANSURANUS: a fuel rod analysis code ready for use, J. Nucl. Mater. 188 (1992) 295–302.

[35] R.L. Williamson, J.D. Hales, S.R. Novascone, M.R. Tonks, D.R. Gaston, C.J. Permann, D. Andrs, R.C. Martineau, Multidimensional multiphysics simulation of nuclear fuel behavior, J. Nucl. Mater. 423 (1–3) (2012) 149–163.

[36] K. Lassmann, A. Schubert, P. Van Uffelen, C. Gyori, J. van de Laar, TRANSURANUS Handbook, Copyright © 1975-2018, Institute for Transuranium Elements, Karlsruhe, 2018.

[37] J.D. Hales, R.L. Williamson, S.R. Novascone, G. Pastore, B.W. Spencer, D.S. Stafford, K.A. Gamble, D.M. Perez, W. Liu, BISON Theory Manual: the Equations behind Nuclear Fuel Analysis, 2016, https://doi.org/10.2172/1374503.

[38] M.S. Veshchunov, On the theory of fission gas bubble evolution in irradiated UO_2 fuel, J. Nucl. Mater. 277 (2000) 67–81.

[39] C. Baker, The migration of intragranular fission gas bubbles in irradiated uranium dioxide, J. Nucl. Mater. 71 (1) (1977) 117–123, https://doi.org/10.1016/0022-3115(77)90195-7.

[40] L. He, X. Bai, J. Pakarinen, B. Jaques, J. Gan, A. Nelson, A. El-Azab, T. Allen, Bubble evolution in Kr-irradiated UO_2 during annealing, J. Nucl. Mater. 496 (2017) 242–250, https://doi.org/10.1016/j.jnucmat.2017.09.036.

[41] R.M. Cornell, An electron microscope examination of matrix fission-gas bubbles in irradiated uranium dioxide, J. Nucl. Mater. 38 (3) (1971) 319–328, https://doi.org/10.1016/0022-3115(71)90061-4.

[42] K. Nogita, K. Une, High resolution TEM of high burnup UO_2 fuel, J. Nucl. Mater. 250 (2–3) (1997) 244–249, https://doi.org/10.1016/S0022-3115(97)00282-1.

[43] K. Nogita, K. Une, High resolution TEM observation and density estimation of Xe bubbles in high burnup UO_2 fuels, Nucl. Instrum. Methods Phys. Res. Sect. B Beam Interact. Mater. Atoms 141 (1) (1998) 481–486, https://doi.org/10.1016/S0168-583X(98)00040-8.

[44] P. Martin, P. Garcia, G. Carlot, C. Sabathier, C. Valot, V. Nassif, O. Proux, J.-L. Hazemann, XAS characterisation of xenon bubbles in uranium dioxide, Nucl. Instrum. Methods Phys. Res. Sect. B Beam Interact. Mater. Atoms 266 (12) (2008) 2887–2891, https://doi.org/10.1016/j.nimb.2008.03.180, radiation Effects in Insulators.

[45] P. Martin, E. Vathonne, G. Carlot, R. Delorme, C. Sabathier, M. Freyss, P. Garcia, M. Bertolus, P. Glatzel, O. Proux, Behavior of fission gases in nuclear fuel: XAS characterization of Kr in UO_2, J. Nucl. Mater. 466 (2015) 379–392, https://doi.org/10.1016/j.jnucmat.2015.08.019.

[46] L. Thomas, Condensed-phase xenon and krypton in UO_2 spent fuel, in: S. Donnelly, J. Evans (Eds.), Fundamental Aspects of Inert Gases in Solids, Plenum Press, New York, 1991, pp. 431–441.

[47] J. Evans, Bubble diffusion to grain boundaries in UO_2 and metals during annealing: a new approach, J. Nucl. Mater. 210 (1994) 21–29.

[48] L. Verma, L. Noirot, P. Maugis, Modelling intra-granular bubble movement and fission gas release during post-irradiation annealing of UO_2 using a meso-scale and spatialized approach, J. Nucl. Mater. 528 (2020) 151874, https://doi.org/10.1016/j.jnucmat.2019.151874.

[49] L.E. Thomas, R.J. Guenther, Characterization of low-gas-release LHR fuels by transmission electron microscopy, MRS Proceedings 127 (1988) 293, https://doi.org/10.1557/PROC-127-293.

[50] R.J. White, A new mechanistic model for the calculation of fission gas release, in: Proceedings of the International Topical Meeting on Light Water Reactor

Fuel Performance, ANS, Palm Beach, Florida, 1994, pp. 196–202.
[51] I. Lifshitz, V. Slyozov, The kinetics of precipitation from supersaturated solid solutions, J. Phys. Chem. Solid. 19 (1–2) (1961) 35–50.
[52] C. Wagner, Theorie der Alterung von Niederschlagen durch Umlosen (Ostwald-Reifung), Zeitschrift Fur Elektrochemie, Berichte der Bunsengesellschaft fur physikalische Chemie 65 (7–8) (1961) 581–591.
[53] A. Baldan, Progress in Ostwald ripening theories and their applications to nickel-base superalloys, J. Mater. Sci. 37 (2002) 2171–2202.
[54] H. Trinkaus, The effect of internal pressure on the coarsening of inert gas bubbles in metals, Scripta Metall. 23 (10) (1989) 1773–1778.
[55] H. Schroeder, P.F. Fichtner, On the coarsening mechanisms of helium bubbles - Ostwald ripening versus migration and coalescence, J. Nucl. Mater. 179–181 (PART 2) (1991) 1007–1010.
[56] H. Schroeder, P. Fichtner, H. Trinkaus, Inert gas bubble coarsening mechanisms, in: S. Donnelly, J. Evans (Eds.), Fundamental Aspects of Inert Gases in Solids, Plenum Press, New York, 1991, pp. 289–297.
[57] P.F. Fichtner, H. Schroeder, H. Trinkaus, A simulation study of Ostwald ripening of gas bubbles in metals accounting for real gas behaviour, Acta Metall. Mater. 39 (8) (1991) 1845–1852.
[58] J. Spino, A.D. Stalios, H. Santa Cruz, D. Baron, Stereological evolution of the rim structure in PWR-fuels at prolonged irradiation: dependencies with burn-up and temperature, J. Nucl. Mater. 354 (1–3) (2006) 66–84.
[59] M.S. Veshchunov, V.E. Shestak, Modelling of fission gas release from irradiated UO_2 fuel under high-temperature annealing conditions, J. Nucl. Mater. 430 (1–3) (2012) 82–89, https://doi.org/10.1016/j.jnucmat.2012.06.048.
[60] S.T. Murphy, A. Chartier, L. Van Brutzel, J.-P. Crocombette, Free energy of Xe incorporation at point defects and in nanovoids and bubbles in $\mathbf{uo}_2$, Phys. Rev. B 85 (2012) 144102, https://doi.org/10.1103/PhysRevB.85.144102.
[61] W. Nixon, D. MacInnes, A model for bubble diffusion in uranium dioxide, J. Nucl. Mater. 101 (1) (1981) 192–199.
[62] M. Veshchunov, V. Shestak, An advanced model for intragranular bubble diffusivity in irradiated UO_2 fuel, J. Nucl. Mater. 376 (2) (2008) 174–180, https://doi.org/10.1016/j.jnucmat.2008.01.026.
[63] R.W. Grimes, C.R.A. Catlow, The stability of fission products in uranium dioxide, Philos. Trans. R. Soc. London, Ser. A: Physical and Engineering Sciences 335 (1639) (1991) 609–634, https://doi.org/10.1098/rsta.1991.0062.
[64] L. Noirot, A method to calculate equilibrium concentrations of gas and defects in the vicinity of an over-pressured bubble in UO_2, J. Nucl. Mater. 447 (1) (2014) 166–178, https://doi.org/10.1016/j.jnucmat.2014.01.011.
[65] L. Verma, L. Noirot, P. Maugis, A new spatially resolved model for defects and fission gas bubbles interaction at the mesoscale, Nucl. Instrum. Methods Phys. Res. Sect. B Beam Interact. Mater. Atoms (October) (2018) 1–8.
[66] J. Spino, J. Rest, W. Goll, C.T. Walker, Matrix swelling rate and cavity volume balance of UO_2 fuels at high burn-up, J. Nucl. Mater. 346 (2–3) (2005) 131–144, https://doi.org/10.1016/j.jnucmat.2005.06.015.
[67] J.A. Turnbull, The distribution of intragranular fission gas bubbles in UO_2 during irradiation, J. Nucl. Mater. 38 (2) (1971) 203–212, https://doi.org/10.1016/0022-3115(71)90044-4.
[68] G. Martin, P. Garcia, C. Sabathier, L. Van Brutzel, B. Dorado, F. Garrido, S. Maillard, Irradiation-induced heterogeneous nucleation in uranium dioxide, Physics Letters, Section A: General, Atomic and Solid State Physics 374 (30) (2010) 3038–3041, https://doi.org/10.1016/j.physleta.2010.05.033.
[69] G. Greenwood, A. Foreman, D. Rimmer, The role of vacancies and dislocations in the nucleation and growth of gas bubbles in irradiated fissile material, J. Nucl. Mater. 1 (4) (1959) 305–324.
[70] F. Ham, Theory of diffusion-limited precipitation, J. Phys. Chem. Solid. 6 (1958) 335–351.
[71] J.A. Turnbull, R.J. White, C. Wise, The diffusion coefficient for fission gas atoms in uranium dioxide, in: International Working Group on Water Reactor Fuel Performance and Technology, Technical Committee on Water Reactor Fuel Element Computer Modelling in Steady State, Transient and Accident Conditions, 1989. Preston, U.K.
[72] S.T. Murphy, P. Fossati, R.W. Grimes, Xe diffusion and bubble nucleation around edge dislocations in UO_2, J. Nucl. Mater. 466 (2015) 634–637, https://doi.org/10.1016/j.jnucmat.2015.09.007.
[73] H. Blank, H.J. Matzke, The effect of fission spikes on fission gas re-solution, Radiat. Eff. 17 (1–2) (1973) 57–64.
[74] R. Nelson, The stability of gas bubbles in an irradiation environment, J. Nucl. Mater. 31 (2) (1969) 153–161.
[75] D. Schwen, M. Huang, P. Bellon, R.S. Averback, Molecular dynamics simulation of intragranular Xe bubble re-solution in UO_2, J. Nucl. Mater. 392 (1) (2009) 35–39, https://doi.org/10.1016/j.jnucmat.2009.03.037.
[76] D. Schwen, R.S. Averback, Intragranular Xe bubble population evolution in UO_2: a first passage Monte Carlo simulation approach, J. Nucl. Mater. 402 (2–3) (2010) 116–123, https://doi.org/10.1016/j.jnucmat.2010.05.006.
[77] K. Govers, C.L. Bishop, D.C. Parfitt, S.E. Lemehov, M. Verwerft, R.W. Grimes, Molecular dynamics study of Xe bubble re-solution in UO_2, J. Nucl. Mater. 420 (1–3) (2012) 282–290, https://doi.org/10.1016/j.jnucmat.2011.10.010.
[78] W. Setyawan, M. W. Cooper, K. J. Roche, R. J. Kurtz, B. P. Uberuaga, D. A. Andersson, B. D. Wirth, Atomistic model of xenon gas bubble re-solution rate due to thermal spike in uranium oxide, J. Appl. Phys. 124 (7). doi:10.1063/1.5042770.
[79] M. Speight, W. Beere, Vacancy potential and void growth on grain boundaries, Met. Sci. 9 (1975) 190–191.
[80] D.R. Olander, Interaction of stresses with inclusions in solids - a review, J. Nucl. Mater. 92 (1980) 163–183.
[81] T. Barani, G. Pastore, D. Pizzocri, D.A. Andersson, C. Matthews, A. Alfonsi, K.A. Gamble, P. Van Uffelen, L. Luzzi, J.D. Hales, Multiscale modeling of fission gas behavior in U_3Si_2 under LWR conditions, J. Nucl. Mater. 522 (2019) 97–110, https://doi.org/10.1016/j.jnucmat.2019.04.037.
[82] N.F. Carnahan, K.E. Starling, Equation of state for nonattracting rigid spheres, J. Chem. Phys. 51 (2) (1969) 635–636, https://doi.org/10.1063/1.1672048.
[83] I.R. Brearley, D.A. MacInnes, An improved equation of state for inert gases at high pressures, J. Nucl. Mater. 95 (3) (1980) 239–252, https://doi.org/10.1016/0022-3115(80)90365-7.
[84] L. Van Brutzel, A. Chartier, A new equation of state for helium nanobubbles embedded in UO_2 matrix calculated via molecular dynamics simulations, J. Nucl. Mater. 518 (2019) 431–439, https://doi.org/10.1016/j.jnucmat.2019.02.015.
[85] A. Jelea, An equation of state for xenon/krypton mixtures confined in the nuclear fuels, J. Nucl. Mater. 530 (2020) 151952, https://doi.org/10.1016/j.jnucmat.2019.151952.
[86] D.A. Andersson, M.R. Tonks, L. Casillas, S. Vyas, P. Nerikar, B.P. Uberuaga, C.R. Stanek, Multiscale simulation of xenon diffusion and grain boundary segregation in UO_2, J. Nucl. Mater. 462 (2015) 15–25, https://doi.org/10.1016/j.jnucmat.2015.03.019.
[87] S.T. Murphy, E.E. Jay, R.W. Grimes, Pipe diffusion at dislocations in UO_2, J. Nucl. Mater. 447 (1–3) (2014) 143–149, https://doi.org/10.1016/j.jnucmat.2013.12.029.
[88] L.K. Mansur, Void swelling in metals and alloys under irradiation: an assessment of the theory, Nucl. Technol. 40 (1) (1978) 5–34, https://doi.org/10.13182/NT78-2.
[89] S. Torquato, Random Heterogeneous Materials: Microstructure and Macroscopic Properties, vol. 82, 2013, https://doi.org/10.1016/j.camwa.2013.03.019 arXiv:1406.6401.
[90] F. Cappia, Investigation of Very High Burnup UO_2 Fuels in Light Water Reactors, Ph.D. thesis, 2017.
[91] S. Torquato, Nearest-neighbor statistics fo packings hard-spheres and disks, Phys. Rev. 51 (4) (1995) 3170–3182.
[92] S. Torquato, B. Lu, J. Rubinstein, Nearest-neighbor distribution functions in many-body systems, Pyhsical Review A 41 (4) (1990) 2059–2075.
[93] D. Pizzocri, T. Barani, L. Luzzi, SCIANTIX: a new open source multi-scale code for fission gas behaviour modelling designed for nuclear fuel performance codes, J. Nucl. Mater. 532 (2020) 152042, https://doi.org/10.1016/j.jnucmat.2020.152042.
[94] P. Van Uffelen, G. Pastore, V. Di Marcello, L. Luzzi, Multiscale modelling for the fission gas behaviour in the TRANSURANUS Code, Nuclear Engineering and Technology 43 (6) (2011) 477–488, https://doi.org/10.5516/NET.2011.43.6.477.
[95] R. Bès, P. Martin, E. Vathonne, R. Delorme, C. Sabathier, M. Freyss, M. Bertolus, P. Glatzel, Experimental evidence of Xe incorporation in Schottky defects in UO_2, Appl. Phys. Lett. 106 (11) (2015) 114102, https://doi.org/10.1063/1.4914300.
[96] K. Nogita, K. Une, Radiation-induced microstructural change in high burnup UO_2 fuel pellets, Nucl. Instrum. Methods Phys. Res. Sect. B Beam Interact. Mater. Atoms 91 (1994) 301–306.
[97] H. Trinkaus, B. Singh, A. Foreman, Mechanisms for decoration of dislocations by small dislocation loops under cascade damage conditions, J. Nucl. Mater. 249 (2–3) (1997) 91–102.
[98] M.S. Veshchunov, V.E. Shestak, Model for evolution of crystal defects in UO_2 under irradiation up to high burn-ups, J. Nucl. Mater. 384 (2009) 12–18, https://doi.org/10.1016/j.jnucmat.2008.09.024.
[99] P.V. Nerikar, D.C. Parfitt, L.A. Casillas Trujillo, D.A. Andersson, C. Unal, S.B. Sinnott, R.W. Grimes, B.P. Uberuaga, C.R. Stanek, Segregation of xenon to dislocations and grain boundaries in uranium dioxide, Phys. Rev. B Condens. Matter 84 (17) (2011) 1–11, https://doi.org/10.1103/PhysRevB.84.174105.
[100] T. Jourdan, Influence of dislocation and dislocation loop biases on microstructures simulated by rate equation cluster dynamics, J. Nucl. Mater. 467 (2015) 286–301, https://doi.org/10.1016/j.jnucmat.2015.09.046.
[101] G. Rossiter, Development of the ENIGMA fuel performance code for whole core analysis ad dry storage assessments, Nuclear Engineering and Technology 43 (6) (2011) 489–498, https://doi.org/10.5516/NET.2011.43.6.489.
[102] T. Kogai, Modelling of fission gas release and gaseous swelling of light water reactor fuels, J. Nucl. Mater. 244 (1997) 131–140, https://doi.org/10.1016/S0022-3115(96)00731-3.